High-p_T pion and kaon production in relativistic nuclear collisions

Yi Zhang and George Fai

Center for Nuclear Research, Department of Physics, Kent State University, Kent, Ohio 44242

Gábor Papp

HAS Research Group for Theoretical Physics, Eötvös University, Pázmány P. 1/A, Budapest 1117, Hungary

Gergely G. Barnaföldi and Péter Lévai

KFKI Research Institute for Particle and Nuclear Physics, P.O. Box 49, Budapest 1525, Hungary

High-p_T pion and kaon production is studied in relativistic proton-proton, proton-nucleus, and nucleus-nucleus collisions in a wide energy range. Cross sections are calculated based on perturbative QCD, augmented by a phenomenological transverse-momentum distribution of partons ("intrinsic k_T"). An energy dependent width of the transverse-momentum distribution is extracted from pion and charged hadron production data in proton-proton/proton-antiproton collisions. Effects of multiscattering and shadowing in the strongly interacting medium are taken into account. Enhancement of the transverse-momentum width is introduced and parameterized to explain the Cronin effect. In collisions between heavy nuclei, the model overpredicts central pion production cross sections (more significantly at higher energies), hinting at the presence of jet quenching. Predictions are made for proton-nucleus and nucleus-nucleus collisions at relativistic heavy ion collider energies.

I. INTRODUCTION

As the bombarding energy is increased, high-p_T particle production becomes a prominent feature of nuclear collisions, as evidenced recently by the data beginning to emerge from the relativistic heavy ion collider (RHIC) [1]. These data call for concentrated theoretical efforts to overcome the challenges presented by the high-energy and many-body features of nuclear collisions at center-of-mass energies of $100A$ GeV$\lesssim\sqrt{s}\lesssim200A$ GeV. Relying on asymptotic freedom, perturbative quantum chromodynamics (PQCD) can be applied at sufficiently high energies. To use PQCD as a practical tool, one takes advantage of the factorization theorem, which provides a simple connection between the level of observed particles and that of the underlying quark-gluon (parton) structure. Briefly, the observable cross sections are expressed in terms of a convolution of partonic cross sections with parton distribution functions (PDFs) and fragmentation functions (FFs), which encode some of the perturbatively noncalculable low-energy aspects of the physics. The resulting calculational scheme adopted here is referred to as the PQCD-improved parton model [2,3]. To assure the validity of a perturbative treatment, we limit the discussion to *hard* particle production, requiring the transverse momentum of the inclusively measured produced particle to be above a certain threshold $p_T\gtrsim p_{T0}$. Typical values of p_{T0} are around 1–3 GeV in the literature.

Hard pion and kaon production in proton-proton (pp) and proton-nucleus (pA) collisions at these energies is in itself of interest, but it is also imperative to study these reactions as a step in the process of understanding hard π and K production in nucleus-nucleus (AA) collisions. The necessity of this systematic approach has been made particularly clear by the high-visibility parallel developments in the subfield of J/ψ

production [4,5]. Significant amounts of experimental data on π and K production in pp collisions are available in the energy range 20 GeV$\lesssim\sqrt{s}\lesssim60$ GeV [6–12]. Higher energies are less thoroughly explored, with mostly calorimetric data on total hadron production (in lieu of the identified pion and kaon spectra at lower energies). In the present paper, we use CERN UA1 [13–15] and Tevatron CDF [16] data from $p\bar{p}\rightarrow h^{\pm}$ reactions to bracket the RHIC energy range from above.

The presence of nuclear effects modifies the predictions of the PQCD-improved parton model for hard particle production in pA collisions, as indicated by available pA hadron production data [6,7,11,17,18]. While hard particle production (usually disregarding nuclear effects) has been used as a testing ground for PQCD, the nuclear modifications are crucially important for RHIC experiments and planned nuclear experiments at the large hadron collider (LHC). In particular, to assess the effects of jet quenching [19–21], precise background calculations and the knowledge of the gluon density of the medium responsible for the energy loss are necessary [22].

In a recent paper [23], we suggested a specific form ("saturation") of the nuclear modification for the cross section enhancement observed at high p_T in pA collisions over what would be expected based on a simple scaling of the appropriate pp cross section (Cronin effect) [6,7]. The present paper provides a more detailed account of our work, incorporating not only neutral but also charged π and K production, with applications and predictions at RHIC energies and for AA collisions. The saturation prescription [23] is looked upon as a limiting case, with the opposite limit corresponding to the participation of all available nucleons in the enhancement of the transverse-momentum width (see

Sec. II B). We study the dependence of the results on the possible choices between these limits, and suggest a connection of the preferred value of the number of semihard (momentum transfer ~ 0.5 GeV) collisions to the results of lower-energy experiments [24–27]. Further measurements are needed to clarify the physical picture, and we argue that the planned pA runs at RHIC [28] are likely to play a very important role in this regard.

A similar effort (with somewhat different emphasis) was published recently [29]. Initial RHIC data and the interest in jet quenching warrant an independent detailed study of the PQCD background to which jet quenching should be applied to achieve agreement with central AA collision data. Our work differs from Ref. [29] on the basic PQCD level in the choice of scales and in the use of the newly published Kniehl, Kramer, and Pötter (KKP) fragmentation functions [30]. Furthermore, we take the position of consistently using leading order (LO) PQCD in the present paper, without introducing a so-called "K factor," which we found to be energy and transverse-momentum dependent in another publication [31]. In this way we have fewer parameters, and the burden of obtaining a good fit to the pp data rests entirely on the transverse-momentum distribution, without mixing the effects of the K factor with those of the intrinsic transverse momentum. We determine the energy-dependent width of the transverse-momentum distribution by fitting pp data, in contrast to the prescribed scale dependence used in Ref. [29].

Our strategy in this paper is to first examine hard pion production in pp collisions up to $\sqrt{s} \lesssim 60$ GeV center-of-mass (c.m.) energy. We find that satisfactory agreement with the data can be achieved in this energy region in LO PQCD, utilizing the width of the intrinsic transverse-momentum distribution of partons in the colliding nucleons. We treat this quantity (also measured in dijet events, see e.g., Ref. [32]), as an energy-dependent nonperturbative parameter. This is discussed in Sec. II A. Having extracted the best value of the transverse-momentum width from the pp data, we apply these ideas to pion production in pA collisions in the same energy range. Our choice for the effective number of semihard collisions is described in Sec. II B. We then discuss AA collisions, and compare our results to CERN data on π^0 production in S+S and Pb+Pb collisions at $\sqrt{s} \sim 20A$ GeV. In Sec. III we move to $K^{\pm}$ production in pp, pA, and AA collisions at the same energies, with the parameters as fixed above. A major step towards calculations at RHIC energies is covered in Sec. IV A, where we attempt to extend the energy range of the parametrization in terms of the width of the transverse-momentum distribution of partons in the nucleon. This is made difficult by the availability of a smaller number of $p\bar{p}$ experiments, most of them at a significantly higher $\sqrt{s}$ than the RHIC energy domain, limited to the measurement of total charged hadron production. The implied uncertainties need to be kept in mind when we display predictions for pA and AA collisions at RHIC energies, in Secs. IV B and IV C, respectively. Section V contains our summary and conclusions. In the Appendix, we discuss the valence and sea contributions to quark fragmentation into charged pions and kaons. We use $\hbar = c = 1$ units.

II. PION PRODUCTION AT CENTER-OF-MASS ENERGIES BELOW ~ 60 GeV

In this section, we first summarize the treatment of particle production in the PQCD-improved parton model, listing various assumptions and ingredients. We introduce the intrinsic transverse-momentum distribution of partons and fit the width of this distribution to available pp data in the energy range 20 GeV$\lesssim \sqrt{s} \lesssim 60$ GeV in Sec. II A. A large body of pion and kaon production data can be utilized in this energy interval to extract information on the width of the transverse-momentum distribution. In Sec. II B the Cronin effect is discussed in pA collisions. Section II C deals with hard pion production in AA collisions.

A. Parton model and PQCD with intrinsic transverse momentum

The invariant cross section for the production of hadron h in a pp collision is described in the PQCD-improved parton model on the basis of the factorization theorem as a convolution [3]

$$E_h \frac{\mathrm{d}\sigma_h^{pp}}{\mathrm{d}^3 p} = \sum_{abcd} \int \mathrm{d}x_a \mathrm{d}x_b \mathrm{d}z_c \; f_{a/p}(x_a, Q^2) f_{b/p}(x_b, Q^2)$$

$$\times \frac{\mathrm{d}\sigma}{\mathrm{d}\hat{t}}(ab \to cd) \frac{D_{h/c}(z_c, Q'^2)}{\pi z_c^2} \hat{s} \delta(\hat{s} + \hat{t} + \hat{u}), \quad (1)$$

where $f_{a/p}(x, Q^2)$ and $f_{b/p}(x, Q^2)$ are the PDFs for the colliding partons a and b in the interacting protons as functions of momentum fraction x, at scale Q, $\mathrm{d}\sigma/\mathrm{d}\hat{t}$ is the hard scattering cross section of the partonic subprocess $ab \to cd$, and the FF, $D_{h/c}(z_c, Q'^2)$ gives the probability for parton c to fragment into hadron h with momentum fraction z_c at scale Q'. We use the convention that the parton-level Mandelstam variables are written with a "hat" (similar to $\hat{t}$ above). The scales are fixed in the present work as $Q = p_T/2$ and $Q' = p_T/(2z_c)$.

In this investigation we use LO partonic cross sections, together with LO PDFs [Glück, Reya, and Vogt (GRV)] [33] and FFs (KKP) [30]. This ensures the consistency of the calculation. An advantage of the GRV parameterization is that this fit uses data down to a rather small scale (≈ 0.25 GeV^2), and thus provides PDFs with approximate validity for hard processes down to relatively small transverse momenta, $p_T \gtrsim p_{T0} = 1$ GeV (with our scale fixing). It can be argued that, to the extent that LO and next-to-leading order (NLO) PDFs and FFs are fitted to the same data, they represent different parametrizations of the same nonperturbative information. However, going to NLO will reduce the scale dependence of PQCD calculations [34]. A NLO study along the lines of the present work is in progress [35]. An alternative approach is to use the "Principle of Minimal Sensitivity" [36] to optimize these scales, as e.g. in Ref. [34]. However, fixing the scales is more convenient as a point of departure for pA and AA studies.

Since the fragmentation functions $D_{h/c}(z_c,Q'^2)$ are normally given for neutral hadrons or equivalently for the combination $h^{\pm}=(h^{+}+h^{-})/2$ (using isospin symmetry), assumptions need to be made to obtain the charge-separated FFs for π^{+}, π^{-}, K^{+}, and K^{-} [37]. These assumptions are connected to the physical picture used to consider fragmentation from valence and sea quarks, respectively. The simplest approximation corresponds to allowing a meson to fragment only from quarks that appear in it as valence contributions. We find this prescription too restrictive, and use a equal division of sea quark contributions between positive and negative mesons in the present work ($\sigma=0.5$), unless indicated otherwise. The value of σ hardly influences pion production, but has a more visible effect on kaons (in particular on K^{-}). We illustrate this by also showing $\sigma=1$ results for comparison in figures with K/π ratios. The details of the approximation are discussed in the Appendix.

The PDFs in Eq. (1) express the probability of finding a parton in the proton with longitudinal momentum fraction x, integrated over transverse momentum up to $k_T=Q$. Recent studies have considered parton distributions unintegrated over the transverse momentum k_T of the parton [38]. In a more phenomenological approach, Eq. (1) can be generalized to incorporate intrinsic transverse momentum by using a product assumption and extending each integral over the parton distribution functions to k_T space [39,40],

$$\mathrm{d}x f_{a/p}(x,Q^2) \rightarrow \mathrm{d}x\,\mathrm{d}^2 k_T g(\vec{k}_T) f_{a/p}(x,Q^2), \qquad (2)$$

where $g(\vec{k}_T)$ is the intrinsic transverse-momentum distribution of the relevant parton in the proton. We follow the phenomenological approach in the present work, taking $g(\vec{k}_T)$ to be a Gaussian

$$g(\vec{k}_T) = \frac{1}{\pi\langle k_T^2 \rangle}\exp[-k_T^2/\langle k_T^2 \rangle]. \qquad (3)$$

Here $\langle k_T^2 \rangle$ is the two-dimensional width of the k_T distribution and it is related to the magnitude of the average transverse momentum of one parton as $\langle k_T^2 \rangle = 4\langle k_T \rangle^2/\pi$. Kinematical details can be found in Refs. [29,39,40]. We note here that endowing the partons with a transverse momentum modifies the definition of the Mandelstam variables $\hat{s}$, $\hat{t}$, and $\hat{u}$. If k_T becomes too large, one of the Mandelstam variables may approach zero, leading to a divergence in the partonic cross section. To regularize this singularity, we follow [39] and earlier studies [41] and make the replacement in the partonic cross section $\mathrm{d}\sigma/\mathrm{d}\hat{t}(ab \rightarrow cd)$ of, e.g., $1/\hat{s} \rightarrow 1/(\hat{s}-M^2)$, where $M=0.8$ GeV is a regulator mass. As discussed in [39], the resultant spectra are sensitive to the choice of M only at $p_T \approx M$, where soft physics becomes important and our PQCD calculations are no longer reliable in any case.

The need for intrinsic transverse momentum in pp collisions was investigated as soon as PQCD calculations were applied to reproduce high-p_T hadron production [2,42]. An average intrinsic transverse momentum of $\langle k_T \rangle \sim 0.3$–$0.4$ GeV could be easily understood in terms of the Heisenberg uncertainty relation for partons inside the proton.
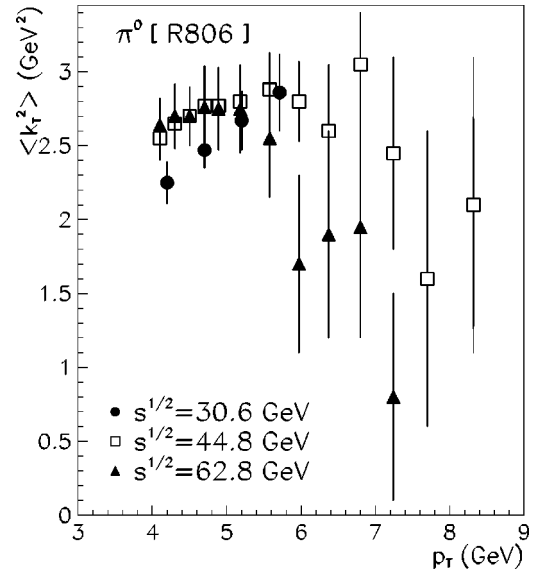

FIG. 1. The width of the transverse-momentum distribution $\langle k_T^2 \rangle$ necessary in Eq. (3) to fit the measured value of the spectrum at the given p_T, point by point, for π^0 production in pp collisions at three energies. The data are from Ref. [8].

However, a larger average transverse momentum of $\langle k_T \rangle \sim 1$ GeV was extracted from jet-jet angular distributions (see, e.g., [32]). Recently, new theoretical efforts were mounted to understand the physical origin of $\langle k_T \rangle$ [38,43,44]. Intrinsic transverse-momentum distributions have been utilized in the contexts of photon production [18,23,45] and J/ψ production [46,47]. The description of deep inelastic scattering in the pomeron framework also appears to require a broad intrinsic k_T distribution [48].

To test the validity of the above approach, we calculated π^0, π^+, and π^- production in pp collisions in the energy range 20 GeV$\lesssim\sqrt{s}\lesssim$60 GeV, and compared the results to data from several independent experiments [7–12]. The calculations were performed using the finite rapidity windows of the data. The Monte Carlo integrals were carried out by the upgraded VEGAS routine [49]. As discussed above, the scales are fixed as $Q=p_T/2$ and $Q'=p_T/(2z_c)$. At each measured transverse-momentum value ($p_T \gtrsim 2$ GeV) we determined the width of the transverse-momentum distribution $\langle k_T^2 \rangle$ necessary to fit the data point at the given p_T, together with its error bar. The values of the extracted $\langle k_T^2 \rangle$ are shown in Fig. 1 for π^0, and in Fig. 2 for π^+ (top panels) and π^- (bottom panels) production. The error bars are determined from the experimental errors.

It is clear from Figs. 1 and 2 that the description of the data in terms of a PQCD calculation augmented by a Gaussian transverse-momentum distribution makes sense only in a limited p_T window in the energy range 20 GeV$\lesssim\sqrt{s}$ $\lesssim$60 GeV. In addition to the requirement of *hard* particle production ($p_T \gtrsim p_{T0}$) imposed for the applicability of PQCD, in most data sets there appears to be an upper limit in transverse momentum, to which $\langle k_T^2 \rangle$ can be extracted with reasonable accuracy. In broad terms, the procedure may be considered sensible for, say 2 GeV$\lesssim p_T \lesssim$7 GeV, depend-
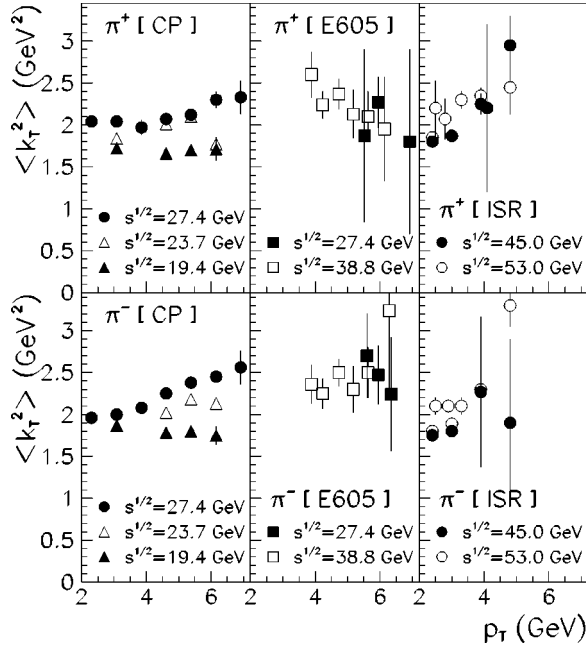
FIG. 2. The width of the transverse-momentum distribution $\langle k_T^2 \rangle$ necessary in Eq. (3) to fit the measured value of the spectrum at the given value of p_T, point by point, for π^+ (top panels) and π^- (bottom panels) production in pp collisions at several energies. The data are from Refs. [7,10–12].

ing on the details of the experiments. Within this window, one may reasonably extract an approximately constant (energy dependent) $\langle k_T^2 \rangle$ for 3 GeV $\lesssim p_T \lesssim 6$ GeV in the full energy range. (Note that the lower limit of the considered p_T interval can be lowered with increasing c.m. energy.) At higher transverse momenta (and fixed $\sqrt{s}$) the effect of intrinsic k_T becomes less important, and thus it is not surprising that, using the error bars on the data, the width $\langle k_T^2 \rangle$ acquires a large uncertainty. Although 3 GeV$\lesssim p_T$ $\lesssim 6$ GeV is a rather narrow transverse-momentum interval, the Cronin effect in pA collisions, to be addressed in the following subsection, is most prominent in this range. This motivated us to use an energy dependent, p_T independent $\langle k_T^2 \rangle$ in what follows, as an approximation.

Concentrating on the above interval in p_T, we next determined the p_T independent $\langle k_T^2 \rangle$ that best fits the pion production data in pp collisions as a function of c.m. energy. In a slight departure from our earlier work [23], we fitted the data minimizing the standard $\chi^2 = \Sigma (\text{Data} - \text{Theory})^2/(\text{Expt.}$ uncertainty)^2 to obtain an optimal $\langle k_T^2 \rangle$ for each energy. Figure 3 summarizes these results. Data are from a range of independent experiments [7–12].

We conclude from this figure that the value of $\langle k_T^2 \rangle$ for hard pion production shows an increasing trend as a function of $\sqrt{s}$ from 20 to 60 GeV (and may be leveling off towards the high-energy end of the interval). The numerical values are significantly larger than expected solely on the basis of the Heisenberg uncertainty principle. It needs to be kept in mind that these values are obtained in the framework of a LO calculation. At NLO, smaller transverse width should be required for the best fit of the data (see some results in Ref.
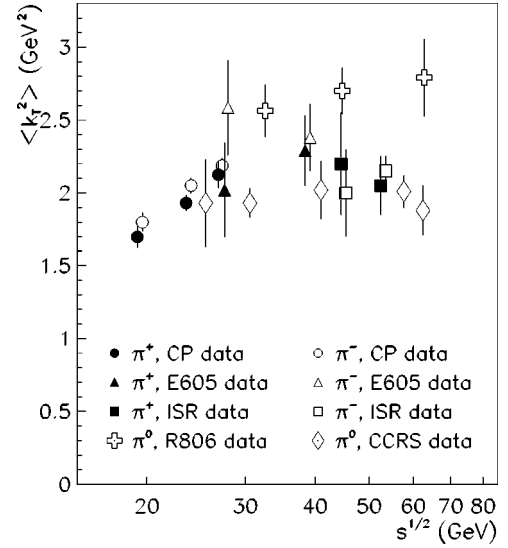

FIG. 3. The best fit values of $\langle k_T^2 \rangle$ in $pp \rightarrow \pi X$ [7–12] reactions, where larger error bars would overlap, the π^- point has been shifted slightly to the right for better visibility.

[31]). At present, we focus on the utility of this parameterization to describe the pp data and view Fig. 3 as a basis for addressing pA and AA collisions at the same level of PQCD.

As an example to illustrate the degree of accuracy of the description in the pp sector, Fig. 4 compares calculated π^+
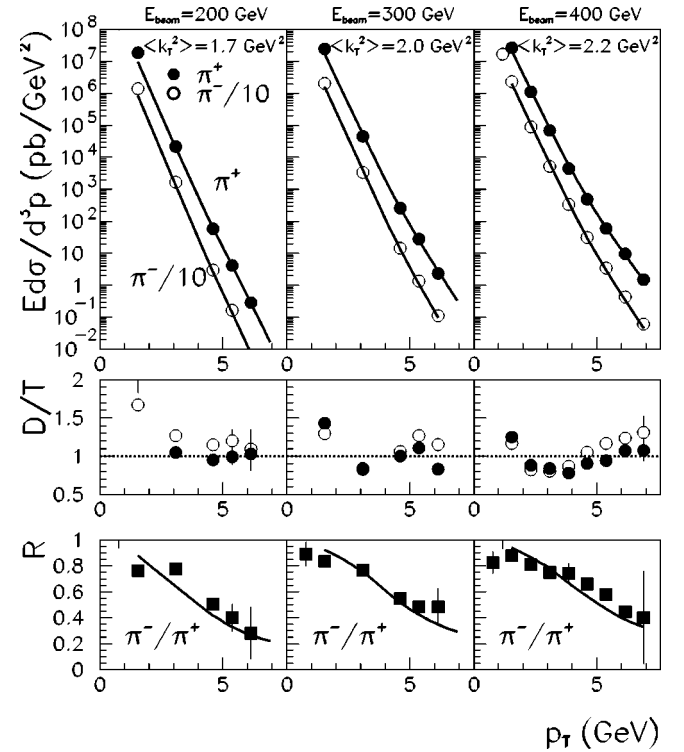

FIG. 4. Invariant cross section of π^+ and π^- production from pp collisions (top row), D/T: data/theory ratios (middle row), and R: π^-/π^+ ratios (bottom row) as functions of transverse momentum at c.m. energies $\sqrt{s} = 19.4$, 23.8, and 27.4 GeV. Data are from [7]. The calculations are carried out in LO, as explained in the text.

and π^- spectra and π^-/π^+ ratios to the data [7] at the c.m. energies $\sqrt{s}=19.4$, 23.8, and 27.4 GeV, respectively, obtained with the values of $\langle k_T^2 \rangle$, indicated in the top panels. We find that the data/theory and π^-/π^+ ratios are well reproduced for 2 GeV $\lesssim p_T \lesssim$ 6 GeV. Based on this and similar examples, we believe that hard pion production in pp collisions is reasonably under control at the present level of calculation. With the parameterization of the transverse-momentum distribution we separated any PQCD uncertainties from the nuclear effects, which we address in the following subsection.

B. Hard pions from proton-nucleus collisions

Interest in the nuclear dependence of hard particle production was triggered by the discovery of the Cronin effect [6,7], and revived with the study of collisions of α particles at the CERN interacting storage ring (ISR) [50–52]. As discussed in the introduction, the nuclear enhancement of hard pion and kaon production cross sections is not only interesting in itself, but we also need to understand these phenomena before we can move to the description of AA collisions at RHIC energies.

The standard framework for addressing high-energy pA collisions is provided by the Glauber model [53,54]. It should be kept in mind, however, that the Glauber model was originally developed with nucleons as elementary constituents, neglecting coherent scattering from several nucleons. Therefore, it is not surprising that refinements to the standard Glauber picture are proposed based on the underlying quark-gluon structure [55–57]. As such modifications are not yet generally accepted or organized into a consistent picture, we continue using the standard Glauber description in the present work.

The key observation for the explanation of the Cronin effect is that in pA collisions, in addition to the hard parton scattering, the incoming and outgoing partons may suffer additional interactions in the presence of the nuclear medium [29,39,40]. An effective way to summarize these additional interactions is in terms of an enhancement of the width of the transverse-momentum distribution above the value in pp collisions, shown in Fig. 3. The extra contribution to the width due to the nuclear environment can be related to the number of nucleon-nucleon collisions in the medium. To characterize the $\langle k_T^2 \rangle$ enhancement, we write the width of the transverse-momentum distribution of the partons in the incoming proton as

$$\langle k_T^2 \rangle_{pA} = \langle k_T^2 \rangle_{pp} + C \cdot h_{pA}(b). \qquad (4)$$

Here $\langle k_T^2 \rangle_{pp}$ is the width of the transverse-momentum distribution of partons in pp collisions from Sec. II A (also denoted simply by $\langle k_T^2 \rangle$), $h_{pA}(b)$ describes the number of *effective* nucleon-nucleon (NN) collisions at impact parameter b that impart an average transverse-momentum squared C. In pA reactions, where one of the partons participating in the hard collision originates in a nucleon with additional NN collisions, we will use the pp width from Fig. 3 for one of

the colliding partons and the enhanced width (4) for the other. The function $h_{pA}(b)$ will be discussed shortly.

According to the Glauber picture, the hard pion production cross section from pA reactions can be written as an integral over impact parameter b

$$E_\pi \frac{d\sigma_\pi^{pA}}{d^3p} = \int d^2b\, t_A(b) E_\pi \frac{d\sigma_\pi^{pp}(\langle k_T^2 \rangle_{pA}, \langle k_T^2 \rangle_{pp})}{d^3p}, \qquad (5)$$

where the proton-proton cross section on the right hand side represents the cross section from Eq. (1) with the transverse extension as given by Eqs. (2) and (3), but with the widths of these distributions as indicated. Here $t_A(b) = \int dz\, \rho(b,z)$ is the nuclear thickness function (in terms of the density distribution ρ) normalized as $\int d^2b\, t_A(b) = A$. Furthermore, it is well known that the PDFs are modified in the nuclear environment ("shadowing") [58,59]. We approximately include shadowing and the isospin asymmetry of heavy nuclei into the nuclear PDFs by considering the average nuclear dependence and using a scale independent parameterization of the shadowing function $S_{a/A}(x)$ adopted from Ref. [58] (see [60]):

$$f_{a/A}(x,Q^2) = S_{a/A}(x)\left[\frac{Z}{A}f_{a/p}(x,Q^2) + \left(1 - \frac{Z}{A}\right)f_{a/n}(x,Q^2)\right], \qquad (6)$$

where $f_{a/n}(x,Q^2)$ is the PDF for the neutron.

The effectivity function $h_{pA}(b)$ can be written in terms of the number of collisions suffered by the incoming proton in the target nucleus $\nu_A(b) = \sigma_{NN} t_A(b)$ where σ_{NN} is the inelastic nucleon-nucleon cross section. Two extreme prescriptions were used for $h_{pA}(b)$ earlier: (i) $h_{pA}^{all}(b) = \nu_A(b) - 1$, corresponding to all NN collisions, except the hard interaction producing the parton to fragment into the observed pion, contributing to the $\langle k_T^2 \rangle$ enhancement [29], and (ii) a "saturated" prescription, where $h_{pA}^{sat}(b)$ was equated to a maximum value of unity whenever $\nu_A(b) \geq \nu_m = 2$ (i.e., it was assumed that only one associated NN collision is responsible for the $\langle k_T^2 \rangle$ enhancement, further collisions are not important in this regard) [23]. In the present work, we examine the dependence of the results on the possible choices between these limits, denoted by $\nu_m = \infty$ and $\nu_m = 2$, respectively. Since even in a heavy nucleus $\nu_A(b)$ does not exceed ≈ 6, we carried out explicit calculations for $2 \leq \nu_m \leq 5$ and without any cut ($\nu_m = \infty$). The coefficient C in Eq. (4) best describing the available pA data [7] for the different values of ν_m is shown at three energies in Fig. 5 as a function of p_T for Be, Ti, and W target nuclei.

For an appealing physical interpretation, the coefficient C is expected to be approximately independent of p_T, of the target used, and probably of beam energy (at least in the energy range studied in Fig. 5). Based on these requirements, we select $\nu_m = 4$ as the value that produces results for C closest to the ideal physical picture. In what follows, we fix $\nu_m = 4$, where the associated value of C is $C = 0.40 \pm 0.05$ GeV^2. This value of C is significantly smaller than what we needed to use in connection to $\nu_m = 2$ earlier (C^{sat},
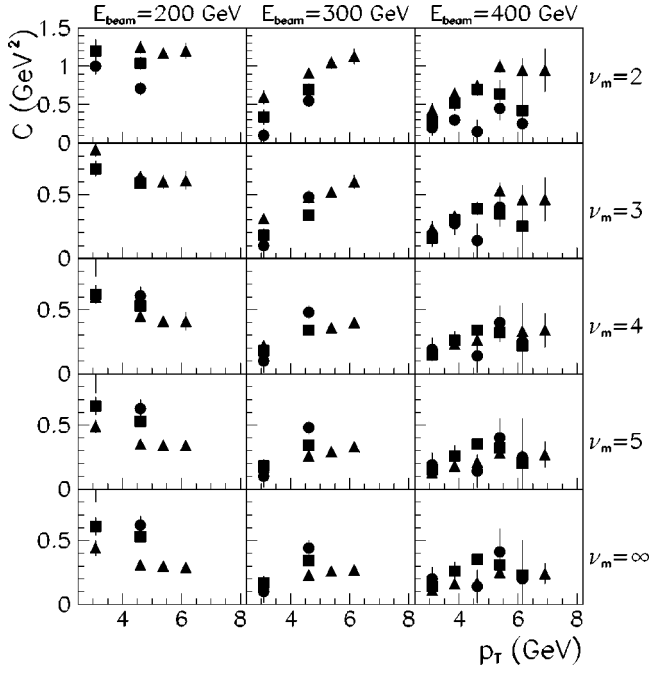
FIG. 5. The best fit values of C in Eq. (4) for Be (dots), Ti (squares), and W (triangles) targets at three different energies as a function of p_T and ν_m. The fitted data are from Ref. [7].

FIG. 6. π^+ spectra and π^-/π^+ ratios from pA collisions for $A=$ Be,Ti,W as functions of transverse momentum at c.m. energies $\sqrt{s}=19.4$, 23.8, and 27.4 GeV. Data are from Ref. [7]. Only pW calculated results for π^-/π^+ shown. Calculated results for the other targets are very similar.

see Ref. [23]), and somewhat larger than would be needed in the case of $\nu_m=\infty$. This can be understood based on the compensating effects of $h_{pA}(b)$ and the value of C in Eq. (4).

It is interesting to note that a similar value for the number of effective inelastic (semihard) collisions was obtained examining nuclear stopping in $p+$ Be,Cu,Au collisions at lower energies ($E_{beam}=12$ and 18 AGeV) [24–26]. The leading proton appeared in these experiments so as not to lose more energy after 2–3 collisions (measured via "gray" tracks from the target). The physics of this phenomenon was connected to the constituent quark picture of the proton, i.e., it was suggested that the state resulting after the inelastic excitation of the three constituent quarks no longer interacts with a high probability. Further experiments are needed to verify this or a similar physical interpretation. Such an effort is in progress at AGS and at CERN SPS (see Refs. [26,27]). Our finding of $\nu_m=4$, which means approximately three effective semihard collisions, overlaps with the above result and points to a similar mechanism, even at higher energies. At this point, the present study lends phenomenological support to the explanation advanced in Refs. [24–26]. Our model is also consistent with the idea proposed by Dokshitzer [61] about the proton being unable to accept more than a characteristic momentum transfer of $Q\approx1$–1.2 GeV. This idea implies the existence of a limiting value of $\langle k_T^2\rangle$ for the proton, which can be accumulated in one or several semihard interactions. Further data are needed at CERN SPS and RHIC energies for a more definitive result. The planned pA collision program at RHIC [28] may play a very important role in this regard.

To illustrate the quality of agreement with the data achieved with the above parametrization, Fig. 6 displays π^+ spectra (upper panels) and π^-/π^+ ratios (lower panels) as functions of p_T, compared to the same pA data [7] as used
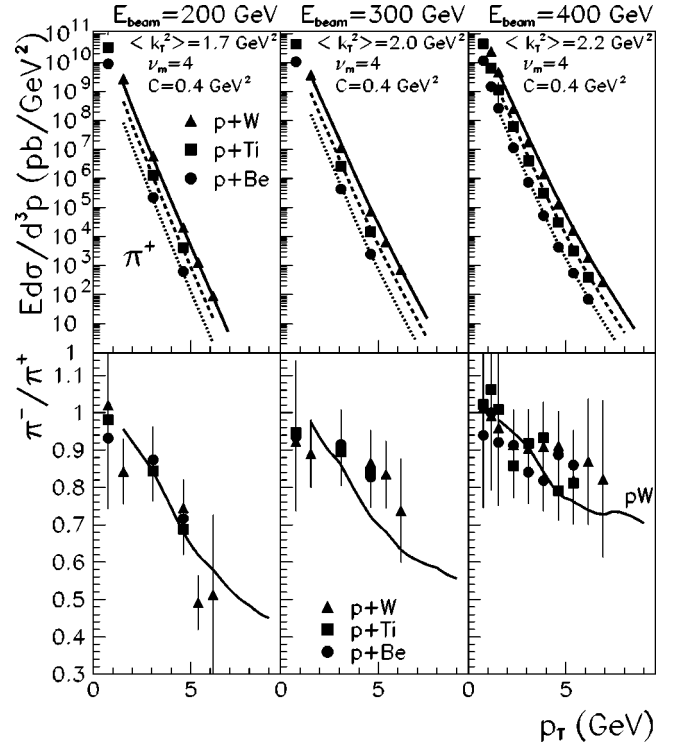
to determine C. The parameters are fixed as indicated in the top panels: $\nu_m=4$, $C=0.4$ GeV^2, and the energy-dependent $\langle k_T^2\rangle_{pp}$ from Fig. 3. There is no observable difference in the π^-/π^+ ratios between the different targets in either the data or the calculated results. (We, therefore, show only the pW calculated results for the π^-/π^+ ratio.)

The Cronin enhancement can be presented in the form of normalized (by mass number A) W/Be cross section ratios [7,11,17]. The data for π^+ and π^- are shown as a function of p_T for the above energies and for $E_{lab}=800$ GeV [11] in Fig. 7, together with the results of calculations with $C=0.35$ GeV^2 (solid line) and with $C=0.45$ GeV^2 (dashed line). The band between these two curves represents the uncertainty in our calculation associated with the extraction of the coefficient C (see Fig. 5).

In the absence of the Cronin effect, these ratios would give a value of identically 1. The significant deviation of the data from unity is therefore a clear confirmation of the nuclear enhancement in the 2 GeV$\lesssim p_T\lesssim6$ GeV transverse-momentum window. At lower p_T, where absorption effects set in, the data indicate a value of the ratio smaller than 1. However, we do not trust our PQCD calculation below $p_T\approx2$ GeV, and thus do not show calculated results for low transverse momenta. At high transverse momenta, where the effects of intrinsic k_T become unimportant as mentioned earlier, the ratio converges to unity in both the data and the calculations.
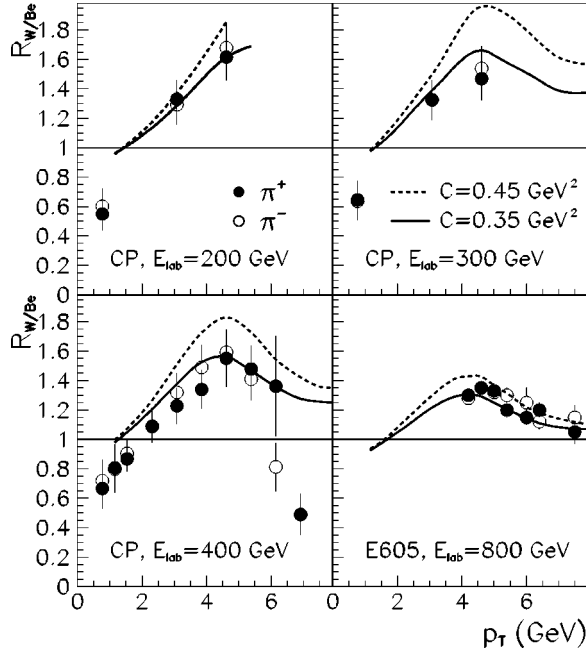
FIG. 7. Normalized W/Be charged pion cross section ratios at four energies. The calculations are carried out with the parameters fixed earlier as discussed in the text. The data are from Refs. [7,10,11]. The deviation from unity represents the Cronin enhancement.

C. Nucleus-nucleus collisions

In nucleus-nucleus reactions [62], where both partons entering the hard collision originate in nucleons with additional semihard collisions, we apply the enhanced width of the parton distribution (4) for both initial partons. Thus,

$$E_\pi \frac{d\sigma_\pi^{AB}}{d^3 p}$$

$$= \int d^2 b \, d^2 r t_A(r) t_B(|\vec{b} - \vec{r}|)$$

$$\times E_\pi \frac{d\sigma_\pi^{pp}(\langle k_T^2 \rangle_{pA}, \langle k_T^2 \rangle_{pB})}{d^3 p}, \qquad (7)$$

where the proton-proton cross section on the right hand side represents the cross section from Eq. (1) with the transverse extension as given by Eqs. (2) and (3), with the enhanced widths of these distributions given by Eq. (4). We emphasize that the parameter values used to describe hard pion production in AA reactions are identical to the ones used earlier in this section for the best description of pion production from pp and pA reactions. In other words, the values of $\langle k_T^2 \rangle_{pp}$ = 1.6 and 1.7 GeV^2, respectively, are taken from Fig. 3 (with a relatively small uncertainty of $\approx \pm 0.1$ GeV at $\sqrt{s}$ ~ 17–20 GeV), and $\nu_m = 4$ and $C = 0.4$ GeV^2 are fixed.

The results of these calculations for central π^0 spectra are compared to the WA80 [63] and WA98 [64] data for S+S, S+Au, and Pb+Pb collisions in Fig. 8 as a function of transverse momentum. Spectra are shown in the top panel, data/
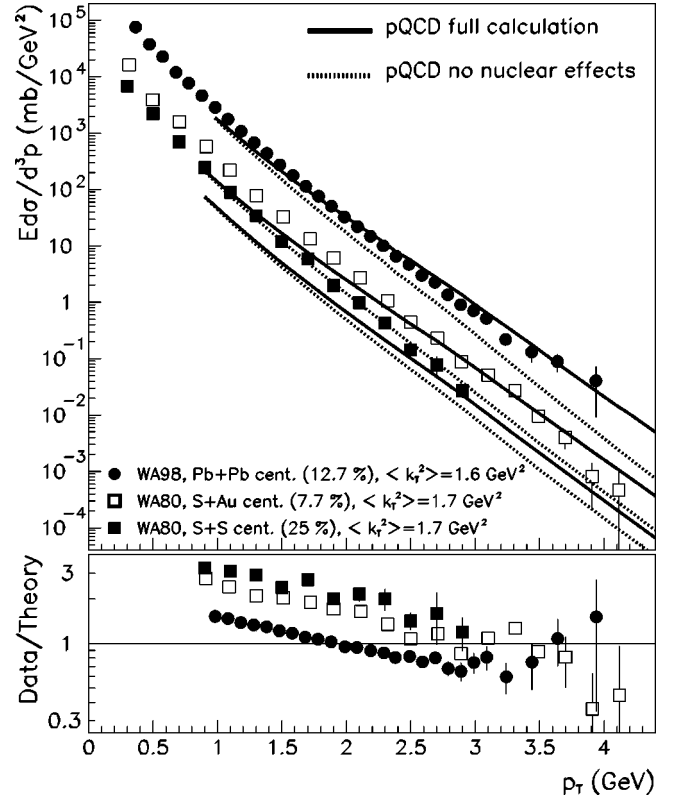

FIG. 8. Neutral pion production compared to data from SPS experiments WA80 [63] and WA98 [64] for central collisions. Calculated invariant cross sections with the nuclear effects turned off (dotted lines) and with the complete model (full lines) are displayed on top together with the corresponding data, data/theory ratios are shown on the bottom (with the full calculation). The parameters are fixed by pp and pA information as discussed in the text.

theory ratios are displayed at the bottom. The dotted lines represent the results of the PQCD calculation with nuclear effects (shadowing and multiscattering) turned off; solid lines correspond to the full calculation. To implement the necessary centrality selection, we represented the nuclei by Woods-Saxon density distributions with radii $R = r_0 A^{1/3}$, with the radius parameter $r_0 = 1.12$ fm and diffuseness a = 0.54 fm. The WA98 experiment measured a total Pb+Pb cross section of 6300 mb, and the centrality cut was made at 12.7% of this total cross section [64]. In our model the same centrality cut is obtained by restricting the impact parameter integration in Eq. (7) to $b_{max} = 5.05$ fm. For S+Au, the measured total cross section of 3600 mb and the experimental centrality cut of 7.7% [63] require $b_{max} = 2.97$ fm in the calculation, while for S+S the total cross section of 1450 mb combined with the 25% centrality cut [63] instruct us to use $b_{max} = 3.4$ fm in our calculation. To test the effect of shadowing, we carried out a calculation with shadowing turned off. Turning off our impact-parameter independent shadowing resulted in a less than 10% shift in the spectra for the central collisions considered at these energies. When comparing to the data, it should be kept in mind that the calculation is intended for *hard* particle production, and it is not expected to describe the data below $p_T \approx 2$ GeV. At low p_T, where soft processes become important, the PQCD model

underestimates the S+S data, as expected. The calculation without nuclear effects (dotted lines) underestimates the data in the entire measured p_T range. The reproduction of the S+S and S+Au data can be considered reasonable for $p_T \gtrsim 2$ GeV, while the Pb+Pb calculation overestimates the data in the same transverse-momentum window by up to 40%. This may be taken as a hint that an additional mechanism is at work in the nuclear medium, which acts to reduce the calculated cross sections. Jet quenching [19–21] is a potential candidate for the physics not included in the present model.

III. HARD KAON PRODUCTION AT CENTER-OF-MASS ENERGIES BELOW ∼60 GeV

In this section we turn to charged kaon production in the same c.m. energy region, using the parameter values fixed in Sec. II. We are interested in the reproduction of kaon data by including the effects of multiscattering and shadowing. Most data are available as kaon to pion ratios; we will display the calculated results in the same manner. Furthermore, as mentioned above, K^- production is particularly sensitive to assumptions made in connection with sea quark fragmentation, discussed in the Appendix. Our standard computations are carried out with the value of $\sigma = 0.5$ for the parameter governing the distribution of sea quarks, but as a reminder to this dependence and to illustrate the sensitivity, we also show calculated results with $\sigma = 1$ in this section.

A. Charged kaons from proton-proton collisions

First we look at kaon spectra and K/π ratios for positive and negative mesons from pp collisions to check if the parametrization introduced for pions is also applicable in this case. Our results are compared to the data [7] in Fig. 9 for K^+ and in Fig. 10 for K^- at the c.m. energies $\sqrt{s} = 19.4$, 23.8, and 27.4 GeV. In the top panels the appropriate pion spectra are also shown as a reference. The kaon cross sections displayed here are calculated with the same value of $\sigma = 0.5$. The data/theory ratios show an agreement similar to that seen in Fig. 4 for pions. In the bottom panels presenting the K/π ratios, full lines correspond to the standard $\sigma = 0.5$, dashed lines depict the calculated results with $\sigma = 1$.

The reproduction of the kaon data from pp collisions can be considered fair, except that in the K/π ratios the apparent structure of the K^+/π^+ ratios is not reproduced, and the peak in the K^-/π^- ratios is shifted to higher transverse momenta and is less pronounced than in the data. It can also be seen that the distribution of sea quarks for the fragmentation of charged mesons, while not too important for the K^+/π^+ ratio, makes a significant difference for K^-/π^-, with $\sigma = 0.5$ describing these ratios better than $\sigma = 1$ for $p_T \lesssim 5$ GeV. If we focus on $p_T > 5$ GeV, the opposite conclusion may be drawn. The sensitivity of the negative ratios to σ is also larger in the $E605$ experimental K/π ratios shown in Fig. 11. Here, measurements extend to higher values of p_T, and $\sigma = 1$ gives a better fit to the K^-/π^- ratios for $p_T \gtrsim 5$ GeV, similarly to the K^-/π^- ratios of Ref. [7]. This may be taken as a hint that our prescription for the fragmen-
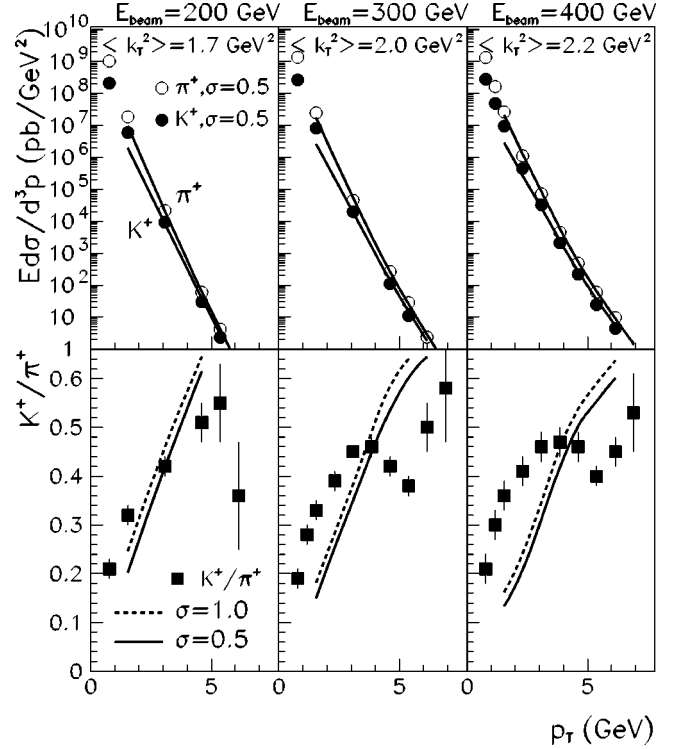

FIG. 9. Spectra of π^+ and K^+ mesons as functions of transverse momentum from pp collisions at c.m. energies $\sqrt{s} = 19.4$, 23.8, and 27.4 GeV (top panels) and K^+/π^+ ratios calculated with $\sigma = 0.5$ (solid) and $\sigma = 1$ (dashed) as explained in the text (bottom panels). Data are from Ref. [7].

tation contribution of sea quarks is too schematic, and σ should be taken p_T dependent in a more realistic calculation.

B. Kaons from proton-nucleus collisions

Next we examine the predictive power of our model for charged kaon production from pA collisions at c.m. energies $\sqrt{s} = 19.4$, 23.8, and 27.4 GeV, with the parameters fixed as above. In other words, $\langle k_T^2 \rangle$ is taken from Fig. 3 as in Sec. III A, and the enhancement of the transverse-momentum width is given by Eq. (4) using $\nu_m = 4$ and $C = 0.4$ GeV^2.

The data are available as K/π ratios, eliminating experimental normalization issues [7]. In Fig. 12 we compare the results of our calculations to these data for Be, Ti, and W targets. K^+/π^+ ratios are shown in the top panels, while K^-/π^- ratios are displayed on the bottom. We present pW calculations with both $\sigma = 0.5$ and $\sigma = 1$. The general tendency of these results and the quality of the agreement between the data and the calculations is very similar to that observed in pp collisions. The deviations increase with energy, but the calculations seem to reflect the gross features of the data. The kaon to pion ratio is not sensitive to the target size. This means that the nuclear enhancement is similar to pions and kaons.

C. Predictions for kaons from nucleus-nucleus collisions

We are not aware of hard kaon data from AA collisions at SPS energies. However, it is natural to extend the present
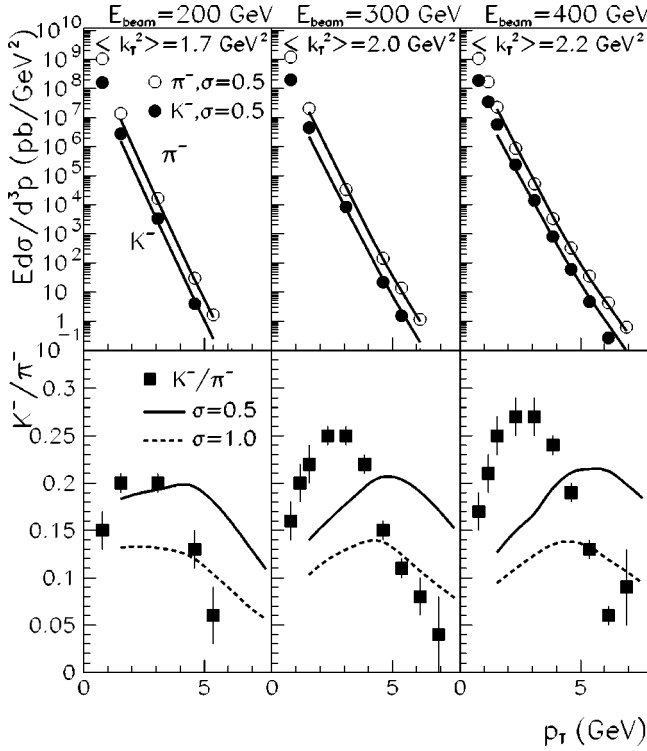
FIG. 10. Spectra of π^- and K^- mesons as functions of transverse momentum from pp collisions at c.m. energies $\sqrt{s} = 19.4$, 23.8, and 27.4 GeV (top panels) and K^-/π^- ratios calculated with $\sigma = 0.5$ (solid) and $\sigma = 1$ (dashed) as explained in the text (bottom panels). Data are from Ref. [7].
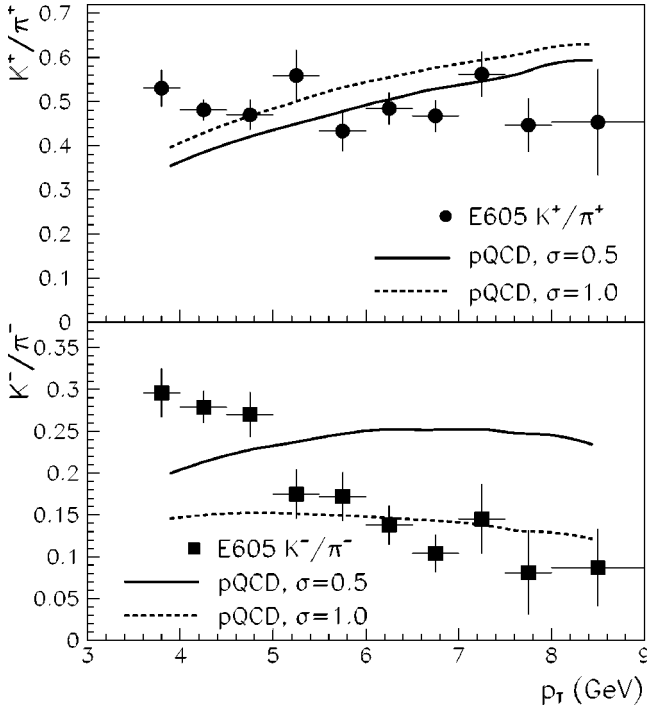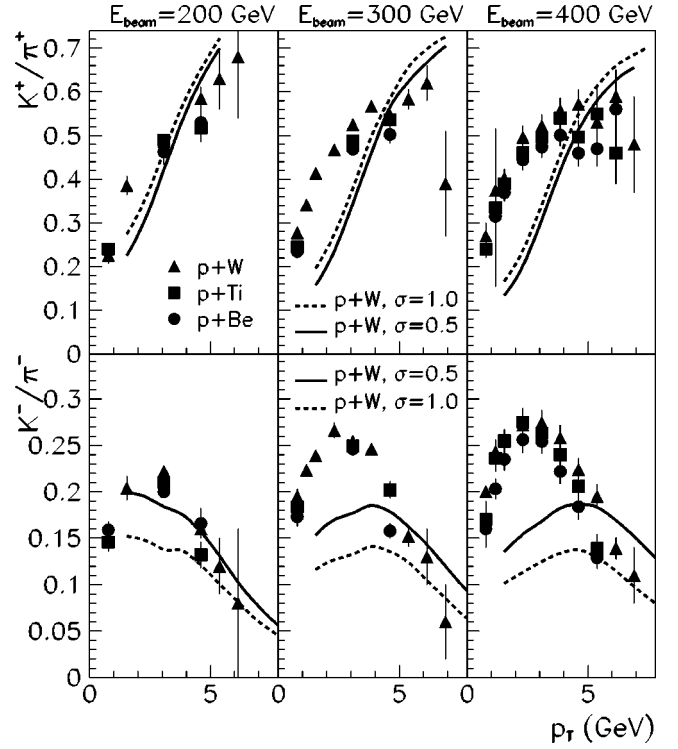

FIG. 12. K^+/π^+ (top) and K^-/π^- (bottom) ratios at c.m. energies $\sqrt{s} = 19.4$, 23.8, and 27.4 GeV. Full lines correspond to $\sigma = 0.5$ and dashed lines display $\sigma = 1$ for pW collisions. (The calculated ratios for the other targets are very similar.) Data are from Ref. [7].

FIG. 11. Ratios of K^+/π^+ (top) and K^-/π^- (bottom) at $E_{beam} = 800$ GeV, calculated with $\sigma = 0.5$ (solid) and $\sigma = 1$ (dashed). Data are from Refs. [10,11].

calculations to kaon production under the conditions of the WA80 and WA98 experiments. Predicted K^+/π^+ (top) and K^-/π^- (bottom) ratios for S+S collisions at $\sqrt{s} = 19.4$ GeV (left panels) and Pb+Pb collisions at $\sqrt{s} = 17.3$ GeV (right panels), as functions of p_T are displayed in Fig. 13.

The appearance of these results is similar to that of the calculated results in the pA case, except that the curves are less steep for AA collisions. Any possible peak at transverse momenta below $p_T = 2$ GeV in the K^-/π^- ratios would be unaccessible for our calculation. Information on these ratios can serve as a test of the present model at SPS energies.

IV. EXTENSION TO RHIC ENERGIES

In preceeding sections, we have developed a description of hard pion and kaon production based on the PQCD-improved parton model, incorporating a phenomenological treatment of the transverse-momentum degree of freedom of the partons. We have seen that a satisfactory agreement with pp data can be achieved up to $\sqrt{s} \approx 60$ GeV, allowing the width of the transverse-momentum distribution $\langle k_T^2 \rangle$ to depend on energy. The available significant body of information on hard pion production in the energy range 20 GeV $\lesssim \sqrt{s} \lesssim 60$ GeV strongly constrains the value of $\langle k_T^2 \rangle$ at lower energies, but the uncertainty increases with $\sqrt{s}$. Modeling the enhancement of the transverse-momentum width associated with additional collisions in the nuclear medium,
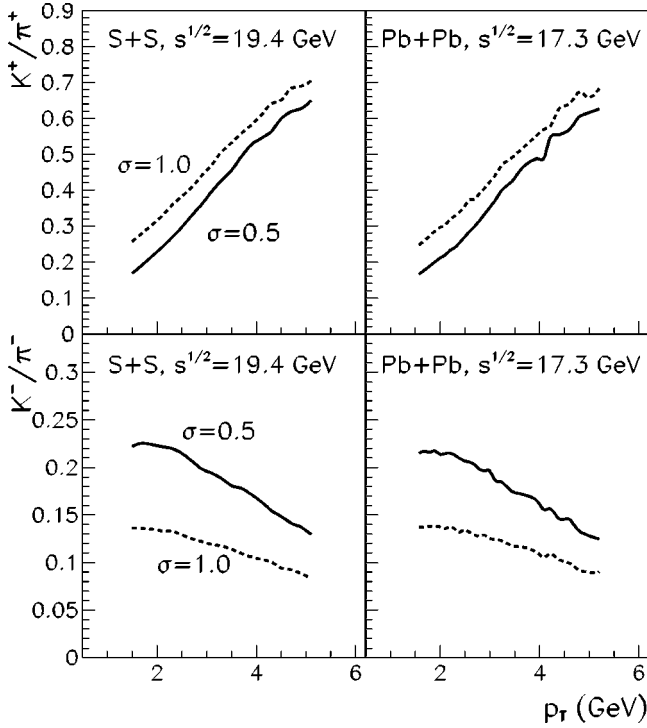
FIG. 13. Predicted K^+/π^+ (top) and K^-/π^- (bottom) ratios for WA80 (S+S at $\sqrt{s} = 19.4$ GeV, left panels), and WA98 (Pb+Pb at $\sqrt{s} = 17.3$ GeV, right panels) experimental conditions. The parameters of the calculation are fixed as discussed in the text. Full lines correspond to $\sigma = 0.5$, dashed lines display results with $\sigma = 1$.

FIG. 14. Top panel: spectra of charged hadrons $(h^+ + h^-)/2$ from $p\bar{p}$ collisions at $\sqrt{s} = 200$, 500, and 900 GeV as calculated with the indicated values of $\langle k_T^2 \rangle$. Bottom panel: data/theory ratios. The data are from the UA1 experiment [14].

we were able to reasonably reproduce hard pion production data from pA and AA reactions in the same energy interval. We then illustrated the use of the model for kaons.

A. Hadron production in $p\bar{p}$ collisions at energies $\sqrt{s} \gtrsim 100$ GeV

In accordance with the main motivation for this study in terms of emerging data and future experiments at RHIC, in this section the parametrization of the pp data will be extended to the RHIC energy region. Unfortunately, we are not aware of useful *identified* hard meson production data from pp or $p\bar{p}$ reactions at energies above $\sqrt{s} \approx 60$ GeV; we have total hadron production data in the form of $(h^+ + h^-)/2$ from CERN UA1 [13–15] and the Tevatron CDF [16]. Since the production of hadrons other than kaons and pions (in particular protons and antiprotons) increases with energy, the accuracy of the extraction of $\langle k_T^2 \rangle$ decreases with increasing energy. Furthermore, we have to face a shortage of data in the energy interval 60 GeV $\lesssim \sqrt{s} \lesssim 500$ GeV.

In Fig. 14 we show the quality of the fit we can achieve with the energy-dependent $\langle k_T^2 \rangle$ to the $(h^+ + h^-)/2$ data from $p\bar{p}$ collisions at $\sqrt{s} = 200$, 500, and 900 GeV [14]. The top panel contains the spectra, the bottom panel gives the data/theory ratios as a function of p_T for the values of $\langle k_T^2 \rangle$ indicated in the top panel.

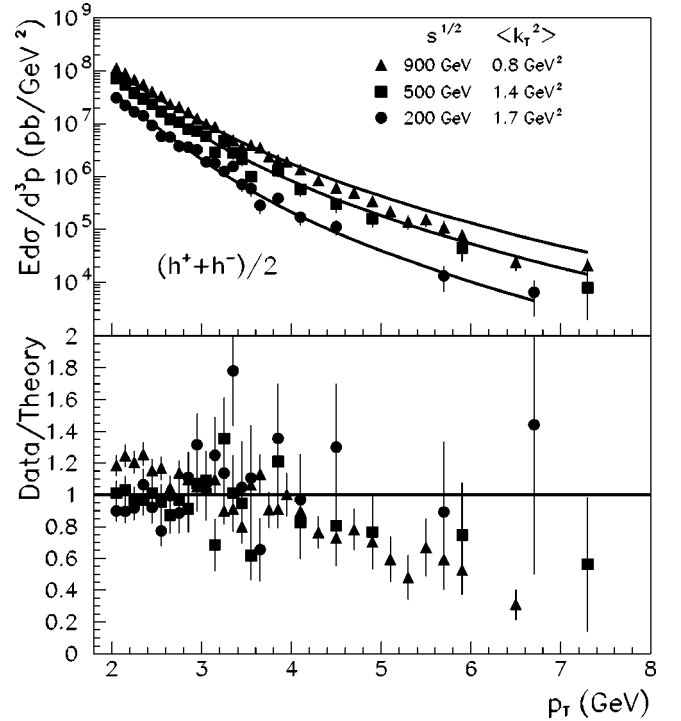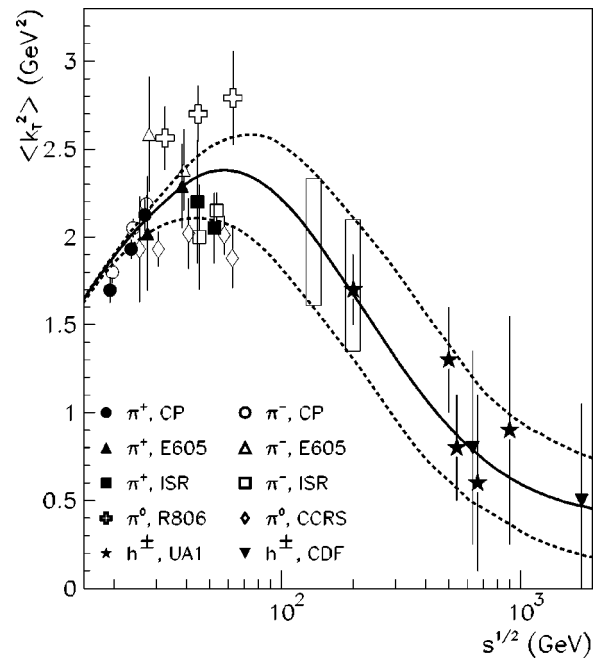Figure 15 summarizes the extracted values of the transverse-momentum width from the $(h^+ + h^-)/2$ data of

FIG. 15. The best fit values of $\langle k_T^2 \rangle$ in $pp \to \pi X$ [7–12] and $p\bar{p} \to h^\pm X$ reactions at $s^{1/2} = 200$, 500, 540, 630, and 900 GeV [13–15] and $s^{1/2} = 630$ and 1800 GeV [16], where large error bars would overlap at the same energy, one of the points has been shifted slightly for better visibility. The band is drawn to guide the eye.

the higher-energy experiments [13–16], together with the points at lower energies extracted from hard *pion* production data (shown earlier in Fig. 3). The solid curve is drawn to guide the eye, and is an attempt to represent the energy dependence of the extracted $\langle k_T^2 \rangle$. The dashed lines delineate an estimated band of increasing uncertainty with increasing $\sqrt{s}$ around this curve. We will use this band to interpolate between the low-energy and high-energy parts of the figure, reading off the $\langle k_T^2 \rangle_{pp}$ values to be applied at RHIC. The rectangular boxes represent an estimate at around $\sqrt{s} = 130$ and 200 GeV, respectively.

It can be seen that $\langle k_T^2 \rangle$ reaches a maximum at around $\sqrt{s} = 60$–100 GeV, with a value of ≈ 2.4 GeV^2. Beyond this energy, the transverse-momentum width necessary to reproduce hadron production data from pp or $p\bar{p}$ reactions at the LO level of the PQCD calculation starts to decrease. The interpolating curve is drawn so that it converges to a small constant value of $\langle k_T^2 \rangle$ as $\sqrt{s} \to \infty$. The high-energy points are based on charged pion and kaon production only, and should be looked upon as upper limits. In the RHIC energy region, we extract $\langle k_T^2 \rangle = 2.0 \pm 0.4$ at $\sqrt{s} \approx 130$ GeV and $\langle k_T^2 \rangle = 1.7 \pm 0.4$ at $\sqrt{s} \approx 200$ GeV for the value of the transverse-momentum width of partons without nuclear enhancement.

For the pA and AA calculations we fixed $\nu_m = 4$ and $C = 0.4$ GeV^2, in lack of a less arbitrary prescription. It needs to be kept in mind, however, that these quantities and the effectivity function $h_{pA}(b)$ of Eq. 4 may well be energy dependent. We carried out computations for pion and kaon production at the RHIC energies of the 2000 run and of the 2001 run of $\sqrt{s} = 130$ GeV and 200 GeV, respectively.

B. Hadron production in pA collisions at RHIC energies

We are now prepared to make certain predictions concerning the planned pA program at RHIC [28]. Since the precise energies and targets to be used are not presently available, we use the c.m. energies of $\sqrt{s} = 130$ and 200 GeV, respectively, and the targets familiar from Sec. II B, as an illustration. For the width of the transverse-momentum distribution of partons in the proton, we take the values $\langle k_T^2 \rangle = 2.0$ GeV^2 and 1.7 GeV^2 at $\sqrt{s} = 130$ and 200 GeV, respectively, representing the centers of the rectangular boxes in Fig. 15. The parameters $\nu_m = 4$ and $C = 0.4$ GeV^2 are fixed. In the top panels of Fig. 16 we show calculated invariant π^0 production cross sections at these energies from collisions of protons with Be, Ti, and W targets. We also include the results of pp calculations as a reference, and the UA1 $p\bar{p}$ data at $\sqrt{s} = 200$ GeV for $h^\pm$ production for comparison [14]. These data were used earlier in Fig. 14. Since kaon production typically does not amount to more than 20% of pion production and the use of antiprotons is not expected to make a significant difference at these energies, the $p + p \to \pi^0 + X$ calculation appears to fit these data on the logarithmic scale almost as well as the earlier $h^\pm$ calculation (see Fig. 14). In the bottom panels of Fig. 16, K^+/π^+ ratios are displayed for the $p + W$ reactions, at the values of $\sigma = 0.5$
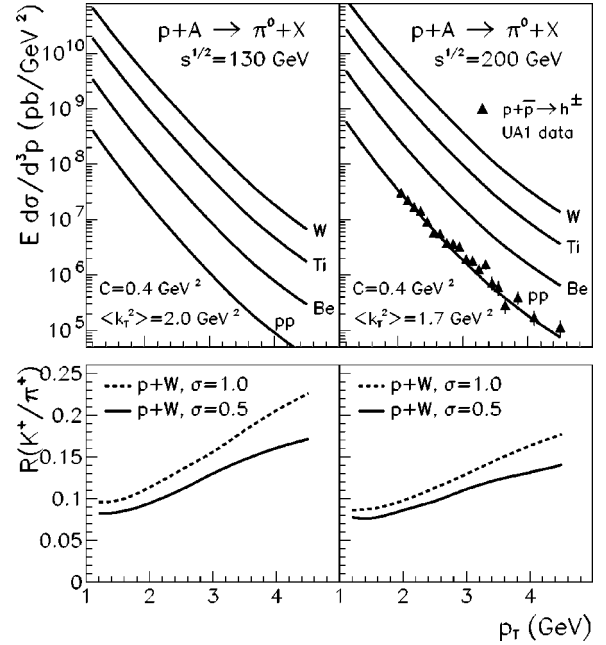

FIG. 16. Top panels: predicted invariant cross sections for π^0 production from $p + $Be, Ti, W collisions at $\sqrt{s} = 130$ GeV (left) and 200 GeV (right). Calculated pp results and the UA1 $h^\pm$ data from $p\bar{p}$ collisions [14] are also included. Bottom panels: predicted K^+/π^+ ratios for $p + W$ collisions with $\sigma = 0.5$ (solid) and $\sigma = 1.0$ (dashed).
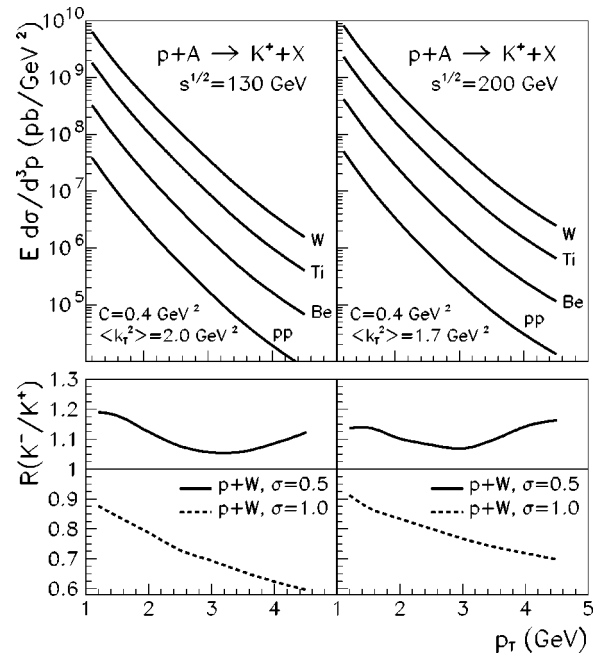

FIG. 17. Top panels: predicted invariant cross sections for K^+ production from $p + $Be, Ti, W collisions at $\sqrt{s} = 130$ GeV (left) and 200 GeV (right). Calculated pp results are also included. Bottom panels: predicted K^-/K^+ ratios for $p + W$ collisions with $\sigma = 0.5$ (solid) and $\sigma = 1.0$ (dashed).
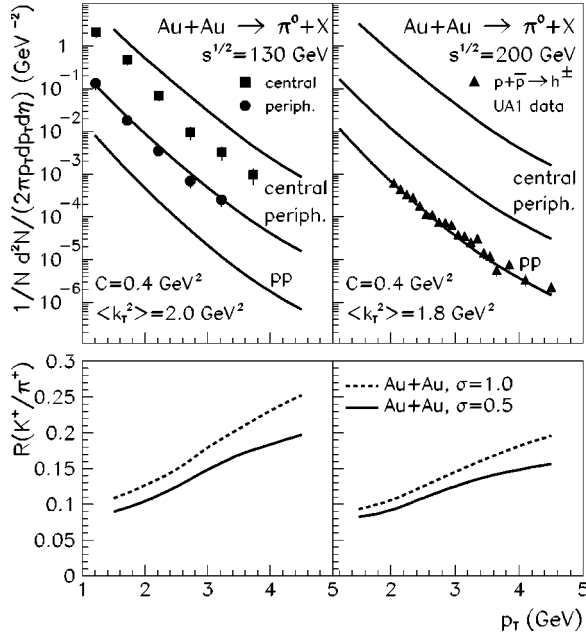
FIG. 18. Top left: calculated central (10%) and peripheral (60–80%) π^0 spectra for Au+Au collision at $\sqrt{s}=130$ GeV, compared to preliminary PHENIX data [65]. We also show the result of our pp calculation. Top right: prediction for central (10%) and peripheral (60–80%) hard π^0 spectra from Au+Au collisions at $\sqrt{s}=200$ GeV. The pp results are included and compared to the UA1 $p\bar{p}$ data at the same energy [14]. Bottom: predicted K^+/π^+ ratios at the same energies.

(solid line) and $\sigma=1.0$ (dashed) for the parameter controlling sea quark fragmentation. These ratios are very similar for the other targets.

Figure 17 displays similar predictions for K^+ production from pA collisions. In the bottom panels we now show K^-/K^+ ratios in $p+W$ collisions for the two values of the parameter σ used earlier. It can be seen from the bottom panels that the value of σ plays a more important role in kaon than in pion production also at these higher energies.

C. Hadron production in Au+Au collisions at RHIC

In the area of AA collisions, calculated high-p_T π^0 production in Au+Au collisions is compared to preliminary PHENIX data at $\sqrt{s}=130$ GeV [65] in the top left panel of Fig. 18; predictions at 200 GeV are displayed on the right of Fig. 18. We use the values $\langle k_T^2 \rangle=2.0$ GeV^2 and 1.7 GeV^2 at $\sqrt{s}=130$ and 200 GeV, respectively, representing the centers of the rectangular boxes in Fig. 15. The parameters $\nu_m=4$ and $C=0.4$ GeV^2 are fixed. Central and peripheral collisions are defined by the top 10% and the 60–80 % bin of the total cross section, corresponding to the experimental selection. With the same radius parameter and diffuseness as used in Sec. II C at SPS energies, this translates to integrals up to $b_{max}=4.7$ fm for central collisions, and from $b_{min}=11.53$ fm to $b_{max}=13.30$ fm for peripheral collisions in Eq. (7). We also show the results of the PQCD calculations of hard pion production from pp collisions for reference. The $p\bar{p}$ data on total charged hadron production at 200 GeV
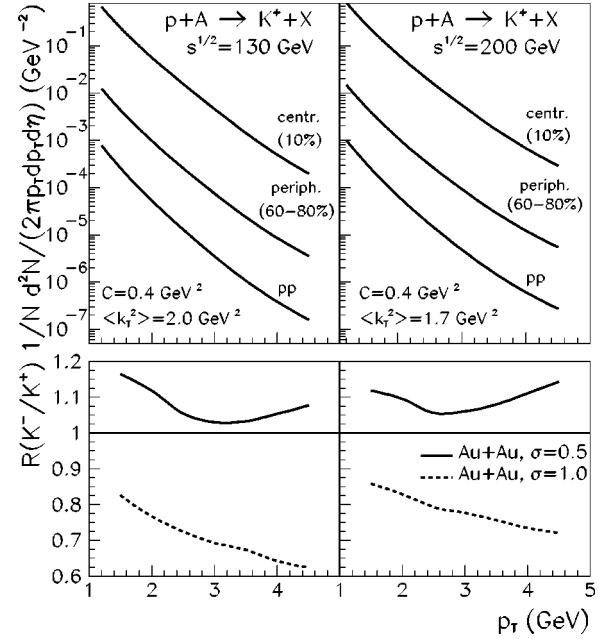
FIG. 19. Predicted K^+ spectra and K^-/K^+ ratios for Au+Au reactions at $\sqrt{s}=130$ GeV (left panels) and 200 GeV (right panels).

[14] are also included in the top right panel of the figure (symbols). In the bottom panels the predicted K^+/π^+ ratios associated with central collisions are displayed. The corresponding peripheral ratios are almost identical to the central ratios shown.

Shadowing is expected to be stronger at RHIC energies than at SPS. Indeed, turning off the impact-parameter independent shadowing indicates that shadowing in itself causes an up to 40% suppression in the 2 GeV$\lesssim p_T \lesssim$6 GeV transverse-momentum range in central collisions at these energies (the effect is decreasing with increasing p_T). Applying an impact-parameter dependent shadowing makes the magnitude of the effect even smaller, in particular for peripheral collisions. Figure 18 shows that the uncertainty introduced by the approximate treatment of shadowing is small compared to the difference between the calculated spectra and the central data.

It can be seen in the top left panel of Fig. 18 that, while our PQCD calculation augmented by nuclear effects approximately reproduces the data on peripheral Au+Au collisions at $\sqrt{s}=130$ GeV, the central data are overestimated by a factor of 3–5. This indicates that an additional mechanism is at work in dense nuclear matter, which would decrease the calculated cross sections at a given p_T. Since this effect can also be looked upon as a shift of the spectra to lower p_T, we speculate that the phenomenon of jet quenching [19–21] is responsible for the discrepancy in central collisions. A study of jet quenching in the present framework is in progress [66].

Figure 19 displays K^+ spectra and K^-/K^+ ratios predicted for the conditions of the $\sqrt{s}=130$ GeV (left panels) and 200 GeV (right panels) RHIC runs, respectively. In the calculations we use the parameter values fixed earlier. It can be seen in the bottom panels that the distribution of sea quarks between K^- and K^+ (governed by the parameter σ) has important implications on the calculated K^-/K^+ ratios.

The predictions in Secs. IV B and IV C above are intended to illustrate the capabilities of the description we have developed. Similar results can be obtained easily for the precise conditions of future RHIC measurements. We find a systematic study of the energy dependence of hard pion and kaon production in pp collisions particularly important. Similarly, a study of the energy and target dependence of pion and kaon production in pA collisions will help pin down the energy dependence of the parameters that characterize the enhancement of the transverse-momentum width in the medium, which have been taken energy independent for the time being.

V. SUMMARY AND CONCLUSION

The commissioning of RHIC opened an exciting new era in nuclear collision physics, with the study of excited strongly interacting matter becoming a reality. It is recognized, however, that a thorough understanding of ultrarelativistic AA collisions presupposes the accurate description of pp and pA collisions in the same framework. In the present paper we attempted to follow the evolution of hard pion and kaon production in relativistic collisions from pp to pA to AA reactions.

The PQCD-improved parton model suggested itself as a natural tool for our study. Of course, PQCD itself is evolving from leading order calculations through the increasing complexity of NLO and NNLO for selected processes. As our major focus in this paper was on the additional physics brought in by pA and AA collisions, it was decided to use LO PQCD throughout. This was supported by evidence that higher-order PQCD does not eliminate the need for the transverse-momentum distribution of partons for a satisfactory fit of pion and kaon production data in pp collisions in the $2 \leqslant p_T \leqslant 6$ GeV window (though the numerical values become smaller, as expected). We used abundant pion production data from pp collisions at c.m. energies $\sqrt{s} \leqslant 60$ GeV to extract the width of the transverse-momentum distribution of partons in the nucleon. The phenomenological value of the description was then tested on kaon production at the same energies.

For the treatment of nuclear systems, we developed a model based on the enhancement of the width of the transverse-momentum distribution of partons in the nuclear medium. An additional parameter was fitted to describe the Cronin effect at these energies. Shadowing and the isospin asymmetry of heavy nuclei were taken into account. We tested the model on charged pion and kaon production. In AA collisions at SPS energies we found an indication of a possible need for an additional mechanism to decrease the calculated cross section of neutral pion production in the collision of heavy nuclei. We speculated that jet quenching may provide that mechanism, beginning to appear already at SPS energies.

Using $p\bar{p}$ data at higher energies, the domain of the extracted transverse-momentum width was extended to cover planned and present RHIC energies. Keeping in mind the rather large uncertainties, predictions were made for pA and AA collisions at RHIC. The overprediction of the preliminary PHENIX data on central π^0 production at $\sqrt{s} = 130$ GeV reinforced our tentative conclusion that additional physics needs to be incorporated in the model to decrease the calculated cross sections when dense nuclear matter is present. Since the disagreement with the central data is much stronger at these energies than at SPS, and jet quenching is expected to increase with energy, jet quenching is a likely candidate for this physics.

Recognizing that the treatment of jet energy loss would require further assumptions and modeling, we leave it for later study. A future treatment of jet quenching in the same framework promises to be of interest as a measure of the gluon density of the medium responsible for the energy loss. We are also interested in a similar study at the NLO level of PQCD.

In conclusion, it appears that a description of pA and AA collisions based on the PQCD-improved parton model augmented by the transverse-momentum distribution of partons and by the nuclear effects of multiscattering and shadowing works reasonably well as a background calculation for hard pion and kaon production at sufficiently high energies and has useful predictive power for the interpretation of present and future RHIC data. A full treatment of nuclear effects will need to take jet energy loss into account. We see our model as a flexible tool to aid in the understanding of the properties of extended strongly interacting matter created at RHIC, LHC, and potential future nuclear colliders.

APPENDIX A: FRAGMENTATION FUNCTIONS FOR CHARGE-SEPARATED PIONS AND KAONS

The parametrization of FFs for pions and kaons is usually given in terms of neutral linear combinations of the charged mesons [30,67], denoted by, e.g., $D_u^{\pi^\pm}$, $D_d^{\pi^\pm}$, and $D_s^{\pi^\pm}$ for pions. Since the present paper focuses attention on separately measured π^+, π^-, K^+, and K^- spectra and their ratios, we need separate FFs for the charged pions and kaons. In this Appendix we describe our approximation used for the charge-separated pion and kaon FFs.

To lowest order, one may assume that each meson species will only fragment from those quarks that appear in it as valence quarks, or from gluons. In this approximation, there is, e.g., no contribution to the fragmentation of pions from strange quarks, or to the fragmentation of kaons from d or $\bar{d}$ quarks. However, these flavors can appear as sea quarks in the respective mesons, and we want to take into account the possibility that pions or kaons fragment from quarks that

appear in them as sea contributions. This implies a separation of the FFs into valence and sea parts, along the lines of Ref. [37]. For consistency, the sea quarks corresponding to the valence flavors in the given meson also need to be considered.

Based on the above ideas, we split the fragmentation functions for pions as

$$D_u^{\pi^\pm} = D_{u,val}^{\pi^\pm} + D_{u,sea}^{\pi^\pm}, \tag{A1}$$

$$D_d^{\pi^\pm} = D_{d,val}^{\pi^\pm} + D_{d,sea}^{\pi^\pm}, \tag{A2}$$

$$D_s^{\pi^\pm} = D_{s,sea}^{\pi^\pm}. \tag{A3}$$

The sea contribution from the fragmentation of a u or d quark can be identified in this case with the FF of the s quark, which appears in the pion only as a sea quark,

$$D_{u,sea}^{\pi^\pm} = D_{d,sea}^{\pi^\pm} = D_{s,sea}^{\pi^\pm} = D_s^{\pi^\pm}. \tag{A4}$$

Furthermore, it is natural to make the usual ansatz connecting the charge-averaged FFs of quarks and antiquarks [37]

$$D_{\bar{u}}^{\pi^\pm} = D_u^{\pi^\pm}, \tag{A5}$$

and similarly for d and s quarks and antiquarks.

The valence contributions to the $\pi^\pm$ FFs can be obtained from the parametrization available in Ref. [30] as

$$D_{u,val}^{\pi^\pm} = D_u^{\pi^\pm} - D_s^{\pi^\pm}, \tag{A6}$$

$$D_{d,val}^{\pi^\pm} = D_d^{\pi^\pm} - D_s^{\pi^\pm}. \tag{A7}$$

Since u and $\bar{d}$ occur in the positive pion as valence quarks, we have

$$D_{u,val}^{\pi^+} = D_{u,val}^{\pi^\pm}, \tag{A8}$$

$$D_{\bar{d},val}^{\pi^+} = D_{\bar{d},val}^{\pi^\pm}, \tag{A9}$$

and similarly for π^-.

The remaining task is to divide the contribution of u quark fragmentation to pions between π^+ and π^- when they appear in the created pion as sea quarks. We propose

$$D_{u,sea}^{\pi^+} = \sigma D_{u,sea}^{\pi^\pm}, \tag{A10}$$

$$D_{u,sea}^{\pi^-} = (1-\sigma) D_{u,sea}^{\pi^\pm}, \tag{A11}$$

$$D_{\bar{u},sea}^{\pi^+} = (1-\sigma) D_{u,sea}^{\pi^\pm}, \tag{A12}$$

$$D_{\bar{u},sea}^{\pi^-} = \sigma D_{u,sea}^{\pi^\pm}, \tag{A13}$$

where $0 \leq \sigma \leq 1$ is a free parameter. It is natural to expect $\sigma = 0.5$ from symmetry arguments. We find that $\sigma = 0.5$ indeed provides a satisfactory description of the available pion data, and use this as the default value in the present paper.

For charged kaons a very similar analysis, with the s quark replacing the d quark as a valence contribution and the d quark playing the role of the contribution that can only arise from the sea, defines the fragmentation functions in an analogous manner.

[1] *Proceedings of Quark Matter 2001* [Nucl. Phys. **A698**, 1 (2002)]; http://www.rhic.bnl.gov/qm2001
[2] J.F. Owens, Rev. Mod. Phys. **59**, 465 (1987).
[3] R.D. Field, *Applications of Perturbative QCD* (Addison-Wesley, Reading, MA, 1995).
[4] H. Satz, Nucl. Phys. (Proc. Suppl.) **94A**, 204 (2001); R. Vogt, hep-ph/0107045.
[5] M.J. Leitch *et al.*, E866/NuSea Collaboration, Phys. Rev. Lett. **84**, 3256 (2000).
[6] J.W. Cronin, H.J. Frisch, M.J. Shochet, J.P. Boymond, P.A. Piroue, and R.L. Sumner (CP), Phys. Rev. D **11**, 3105 (1975).
[7] D. Antreasyan, J.W. Cronin, H.J. Frisch, M.J. Shochet, L. Kluberg, P.A. Piroue, and R.L. Sumner (CP), Phys. Rev. D **19**, 764 (1979).
[8] C. Kourkoumelis *et al.*, R806 Collaboration, Z. Phys. C **5**, 95 (1980).
[9] F.W. Büsser *et al.*, CCRS Collaboration, Nucl. Phys. **B106**, 1 (1976).
[10] D.E. Jaffe *et al.*, E605 Collaboration, Phys. Rev. D **40**, 2777 (1989).
[11] P.B. Straub *et al.*, Phys. Rev. Lett. **68**, 452 (1992).
[12] B. Alper *et al.*, ISR Collaboration, Nucl. Phys. **B100**, 237 (1975).

[13] G. Arnison *et al.*, UA1 Collaboration, Phys. Lett. **118B**, 167 (1983).
[14] C. Albajar *et al.*, UA1 Collaboration, Nucl. Phys. **B335**, 261 (1990).
[15] C. Bocquet *et al.*, UA1 Collaboration, Phys. Lett. B **366**, 434 (1996).
[16] F. Abe *et al.*, CDF Collaboration, Phys. Rev. Lett. **61**, 1819 (1988).
[17] C.N. Brown *et al.*, Phys. Rev. C **54**, 3195 (1996).
[18] L. Apanasevich *et al.*, E706 Collaboration, Phys. Rev. Lett. **81**, 2642 (1998); Phys. Rev. D **63**, 014009 (2000).
[19] M. Gyulassy and M. Plümer, Phys. Lett. B **243**, 432 (1990); X.-N. Wang and M. Gyulassy, Phys. Rev. Lett. **68**, 1480 (1992).
[20] R. Baier, Yu.L. Dokshitzer, A.H. Mueller, and D. Schiff, Nucl. Phys. **B531**, 403 (1998); R. Baier, D. Schiff, and B.G. Zakharov, Annu. Rev. Nucl. Part. Sci. **50**, 37 (2000).
[21] M. Gyulassy, P. Lévai, and I. Vitev, Phys. Rev. Lett. **85**, 5535 (2000); Nucl. Phys. **B594**, 371 (2001).
[22] M. Gyulassy, I. Vitev, and X.-N. Wang, Phys. Rev. Lett. **86**, 2537 (2001); X.-N. Wang and M. Gyulassy, *ibid.* **86**, 3496 (2001).
[23] G. Papp, P. Lévai, and G. Fai, Phys. Rev. C **61**, 021902(R) (2000).

[24] B. Cole *et al.*, E910 Collaboration, Nucl. Phys. **A661**, 366 (1999).

[25] I. Chemakin *et al.*, E910 Collaboration, Phys. Rev. Lett. **85**, 4868 (2000); nucl-ex/0108007.

[26] B. Cole, Nucl. Phys. **A698**, 1 (2002); http://www.rhic.bnl.gov/qm2001

[27] G. Veres, NA49 Collaboration (unpublished).

[28] S. Aronson *et al.*, http://www.bnl.gov/rhic/townmeeting/agenda_b.htm

[29] X.N. Wang, Phys. Rev. C **61**, 064910 (2001).

[30] B.A. Kniehl, G. Kramer, and B. Pötter, Nucl. Phys. **B597**, 337 (2001); hep-ph/0011155.

[31] G.G. Barnaföldi, G. Fai, P. Lévai, G. Papp, and Y. Zhang, J. Phys. G **27**, 1767 (2001).

[32] M.D. Corcoran *et al.*, E609 Collaboration, Phys. Lett. B **259**, 209 (1991).

[33] M. Glück, E. Reya, and A. Vogt, Z. Phys. C **53**, 127 (1992).

[34] P. Aurenche, M. Fontannaz, J.Ph. Guillet, B. Kniehl, E. Pilon, and M. Werlen, Eur. Phys. J. C **9**, 107 (1999); P. Aurenche, M. Fontannaz, J.Ph. Guillet, B. Kniehl, and M. Werlen, *ibid.* **13**, 347 (2001).

[35] G. Papp, Y. Zhang, G. Fai, G.G. Barnaföldi, and P. Lévai (unpublished).

[36] P.M. Stevenson, Phys. Rev. D **23**, 2916 (1981).

[37] J. Binnewies, B.A. Kniehl, and G. Kramer, Z. Phys. C **65**, 471 (1995).

[38] M.A. Kimber, A.D. Martin, and M.G. Ryskin, Eur. Phys. J. C **12**, 655 (2000); hep-ph/0101348 (2001).

[39] X.N. Wang, Phys. Rep. **280**, 287 (1997); Phys. Rev. Lett. **81**, 2655 (1998); Phys. Rev. C **58**, 2321 (1998).

[40] C.Y. Wong and H. Wang, Phys. Rev. C **58**, 376 (1998).

[41] R.P. Feynman, R.D. Field, and G.C. Fox, Nucl. Phys. **B128**, 1 (1977); Phys. Rev. D **18**, 3320 (1978).

[42] D. Sivers, S. Brodsky, and R. Blankenbecler, Phys. Rep. **23**, 1 (1976); A.P. Contogouris, R. Gaskell, and S. Papadopoulos, Phys. Rev. D **17**, 2314 (1978).

[43] X. Guo and J. Qiu, Phys. Rev. D **53**, 6144 (1996).

[44] H.L. Lai and H.N. Li, Phys. Rev. D **58**, 114020 (1998).

[45] J. Huston *et al.*, Phys. Rev. D **51**, 6139 (1995).

[46] K. Sridhar, A.D. Martin, and W.J. Stirling, Phys. Lett. B **438**, 211 (1998).

[47] P. Zhuang and J. Hüfner, nucl-th/0109037.

[48] N.N. Nikolaev, hep-ph/9905562.

[49] R. Kreckel, physics/9812011; G.P. Lepage, J. Comput. Phys. **27**, 192 (1978).

[50] J.H. Kühn, Phys. Rev. D **13**, 2948 (1976).

[51] U.P. Sukhatme and G. Wilk, Phys. Rev. D **25**, 1978 (1982).

[52] M. Lev and B. Petersson, Z. Phys. C **21**, 155 (1983).

[53] R.J. Glauber, in *Lectures in Theoretical Physics*, edited by W.E Brittin and L.G. Dunham (Interscience, New York, 1959), Vol. 1, p. 315; R.J. Glauber and G. Matthiae, Nucl. Phys. **B21**, 135 (1970).

[54] V.N. Gribov, Sov. J. Nucl. Phys. **30**, 709 (1970).

[55] T. Peitzmann, Phys. Lett. B **450**, 7 (1999).

[56] C. Gale, S. Jeon, and J. Kapusta, Phys. Rev. Lett. **82**, 1636 (1999).

[57] J. Hüfner, B. Kopeliovich, and A. Polleri, hep-ph/0012010; Eur. Phys. J. A **11**, 457 (2001); A. Polleri, nucl-th/0002054.

[58] X.N. Wang and M. Gyulassy, Phys. Rev. D **44**, 3501 (1991).

[59] K.J. Eskola, V.J. Kolhinen, and C.A. Salgado, Eur. Phys. J. C **9**, 61 (1999).

[60] After completing the present calculations, a new shadowing parametrization, treating quarks and gluons separately, came to our attention: S. Li and X.N. Wang, nucl-th/0110075. We checked the effect of the new parametrization at $\sqrt{s}$ =18 GeV, and found a difference of a few percent, which would not change the physics results presented here.

[61] Yu.L. Dokshitzer, Philos. Trans. R. Soc. London, Ser. A **359**, 309 (2001).

[62] These are denoted by *AA* in the text, even though not all studied systems are symmetric.

[63] R. Albrecht *et al.*, WA80 Collaboration, Phys. Lett. B **361**, 14 (1995).

[64] M.M. Aggarwal *et al.*, WA98 Collaboration, Phys. Rev. Lett. **85**, 3595 (2000); T. Peitzmann (private communication); nucl-ex/0006007; nucl-ex/0108006.

[65] G. David, PHENIX Collaboration, Nucl. Phys. **A698**, 227 (2002); http://www.rhic.bnl.gov/qm2001

[66] P. Levai, G. Papp, G. Fai, and M. Gyulassy, nucl-th/0012017; P. Levai, G. Papp, G. Fai, M. Gyulassy, G.G. Barnaföldi, I. Vitev, and Y. Zhang, Nucl. Phys. **A698**, 631 (2002); nucl-th/0104035.

[67] J. Binnewies, B.A. Kniehl, and G. Kramer, Phys. Rev. D **52**, 4947 (1995).